Homogeneous Atomic Fermi Gases

Biswaroop Mukherjee,[1] Zhenjie Yan,[1] Parth B. Patel,[1] Zoran Hadzibabic,[1,2] Tarik Yefsah,[1,3] Julian Struck,[1] and Martin W. Zwierlein[1]

[1]*MIT-Harvard Center for Ultracold Atoms, Research Laboratory of Electronics, and Department of Physics, Massachusetts Institute of Technology, Cambridge, Massachusetts 02139, USA*

[2]*Cavendish Laboratory, University of Cambridge, J. J. Thomson Avenue, Cambridge CB3 0HE, United Kingdom*

[3]*Laboratoire Kastler Brossel, CNRS, ENS-PSL Research University, UPMC-Sorbonne Universités and Collège de France, Paris 75005, France*

(Received 31 October 2016; published 23 March 2017)

We report on the creation of homogeneous Fermi gases of ultracold atoms in a uniform potential. In the momentum distribution of a spin-polarized gas, we observe the emergence of the Fermi surface and the saturated occupation of one particle per momentum state: the striking consequence of Pauli blocking in momentum space for a degenerate gas. Cooling a spin-balanced Fermi gas at unitarity, we create homogeneous superfluids and observe spatially uniform pair condensates. For thermodynamic measurements, we introduce a hybrid potential that is harmonic in one dimension and uniform in the other two. The spatially resolved compressibility reveals the superfluid transition in a spin-balanced Fermi gas, saturation in a fully polarized Fermi gas, and strong attraction in the polaronic regime of a partially polarized Fermi gas.

DOI: 10.1103/PhysRevLett.118.123401

Ninety years ago, Fermi derived the thermodynamics of a gas of particles obeying the Pauli exclusion principle [1]. The Fermi gas quickly became a ubiquitous paradigm in many-body physics; yet even today, Fermi gases in the presence of strong interactions pose severe challenges to our understanding. Ultracold atomic Fermi gases have emerged as a flexible platform for studying such strongly correlated fermionic systems [2–6]. In contrast to traditional solid state systems, quantum gases feature tunable spin polarization, dimensionality, and interaction strength. This enables the separation of quantum statistical effects from interaction-driven effects, and invites the exploration of rich phase diagrams, for example bulk Fermi gases in the BEC-BCS crossover [3–10] and Fermi-Hubbard models in optical lattices [11–20].

So far, Fermi gas experiments have been performed in inhomogeneous traps, where the nonuniform density leads to spatially varying energy and length scales. This poses a fundamental problem for studies of critical phenomena for which the correlation length diverges. Furthermore, in a gas with spatially varying density, a large region of the phase diagram is traversed, potentially obscuring exotic phases that are predicted to occur in a narrow range of parameters. This is most severe for supersolid states, such as the elusive FFLO state [21–23], where the emergent spatial period is well defined only in a homogeneous setting. A natural solution to these problems is the use of uniform potentials, which have recently proved to be advantageous for thermodynamic and coherence measurements with Bose gases [24–27].

Here, we realize homogeneous Fermi gases in a versatile uniform potential. For spin-polarized gases, we observe both the formation of the Fermi surface and the saturation at one fermion per momentum state, due to Pauli blocking. Spatially uniform pair condensates are observed for spin-balanced gases, offering strong prospects for the exploration of long-range coherence, critical fluctuations, and supersolidity.

In cases where the local density approximation (LDA) is valid, the spatially varying local chemical potential in an inhomogeneous trap can be utilized for thermodynamic [28–31] and spectroscopic [7,32,33] measurements. However, reconstructing the local density from line-of-sight integrated density profiles typically increases noise, while spatially selecting a central region of the gas reduces signal. A potential that is uniform along the line-of-sight is the natural solution. Combining the desirable features of homogeneous and spatially varying potentials, we introduce a hybrid potential that is uniform in two dimensions and harmonic in the third. The line-of-sight integration is now turned into an advantage: instead of averaging over a wide region of the phase diagram, the integration yields a higher signal-to-noise measurement of the local density. Using this geometry, we observe the characteristic saturation of isothermal compressibility in a spin-polarized gas, while a strongly interacting spin-balanced gas features a peak in the compressibility near the superfluid transition [31].

In our experiment, we prepare atoms in the two lowest hyperfine states of ^{6}Li near a Feshbach resonance, and load them into the uniform potential of the optical box trap depicted in Fig. 1(a), after evaporative precooling in a crossed dipole trap. We typically achieve densities and Fermi energies of up to $n \approx 10^{12}$ cm^{-3} and $E_F \approx h \times 13$ kHz, corresponding to $\sim 10^6$ atoms per spin state in the box. The lifetime of the

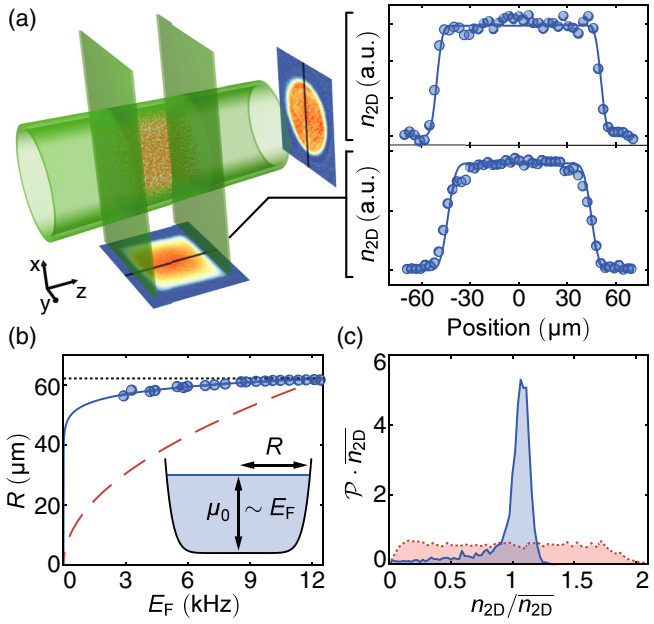

FIG. 1. Homogeneous Fermi gas. (a) Schematic of the box trap and cuts through the column-integrated density profiles along the axial and radial directions. (b) Radius of the cloud as a function of the Fermi energy. The dotted black and dashed red lines correspond to a perfect box potential and a harmonic potential, respectively, and are scaled to converge at the highest E_F. The blue solid line corresponds to a power law potential $V(r) \sim r^{16}$. (c) Measured radial probability density $\mathcal{P}(n_{2D})$ for the column-integrated density n_{2D}, averaging about 20 in-trap images. The blue solid and red dashed lines correspond to the uniform and Gaussian traps, respectively.

Fermi gas in the box trap is several tens of seconds. The uniform potential is tailored using blue-detuned laser light for the confining walls. The sharp radial trap barrier is provided by a ring beam generated by an axicon [34,35], while two light sheets act as end caps for the axial trapping [36]. Furthermore, the atoms are levitated against gravity by a magnetic saddle potential [3]. The residual radial anticonfining curvature of the magnetic potential is compensated optically, while an axial curvature results in a weak harmonic potential described by a trapping frequency of $\omega_z = 2\pi \times 23.9$ Hz. This typically results in a variation of the potential along the axial direction that is less than 5% of the Fermi energy. Note that the magnetic moments of the two spin states of ^{6}Li differ by less than 0.1% at unitarity, resulting in a negligible difference in trapping potentials. We characterize the steepness of the trap walls by measuring the radial extent R of the cloud as a function of Fermi energy [see Fig. 1(b)]. Modeling the trap walls with a power law potential, we obtain $V(r) \sim r^{16.2\pm1.6}$ [36].

A stringent measure of the homogeneity of the gas is the probability distribution $\mathcal{P}(n)$ for the atomic density n. Imaging along the z and x directions yields the radial and axial probability distribution $\mathcal{P}(n_{2D})$ for the column density n_{2D} (see Fig. 1(c) and Ref. [36]). The distribution for the homogeneous gas is sharply peaked near the trap average density $\overline{n_{2D}}$. For comparison, we also show $\mathcal{P}(n_{2D})$ for an optical Gaussian trap, which is spread over a large range of densities.

Fermions at low temperatures are characterized by Pauli blocking [1]. Consequences of Pauli blocking have been observed in ultracold gases, for example, in nondegenerate samples, the reduction of collisions in spin-polarized gases below the p-wave threshold [2,37] and, upon entering degeneracy, Pauli pressure [38,39], reduced collisions [40,41], antibunching in noise correlations [42], and the reduction of density fluctuations [43,44]. In optical lattices under microscopes, Pauli blocking has been observed in real space through observations of band insulating states [16,17,45] and of the Pauli hole in pair correlations [20]. Typically obscured in the time of flight expansion of an inhomogeneous atomic gas, the Fermi surface has been observed by probing only the central region of a harmonically trapped gas [46]. Now, the uniform box potential enables us to directly observe the consequence of Pauli blocking in momentum space for degenerate gases: the Fermi-Dirac momentum distribution, featuring the emergence of a Fermi surface near the Fermi wave vector k_F and the saturated occupation of momentum states below k_F to one particle per momentum cell.

To measure the momentum distribution $f(\mathbf{k})$, we release a highly spin-imbalanced gas ($n_\downarrow/n_\uparrow < 0.05$, where $n_\uparrow$ and $n_\downarrow$ are the densities of the majority and minority spin components, respectively) from the uniform potential into the small residual axial harmonic potential (along the z axis). To ensure the ballistic expansion of the gas, the minority component is optically pumped into a weakly interacting state within 5 μs [36]. After a quarter period of expansion in the harmonic trap, the axial momenta k_z are mapped into real space via $z = \hbar k_z/m\omega_z$ [47–50]. In contrast to conventional time of flight measurements, this method is unaffected by the in-trap size of the gas. The measured integrated density profile $n_{1D}(z) = \iint dxdyn(x,y,z)$ reflects the integrated momentum distribution $f_{1D}(k_z) = (2\pi)^{-2}\iint dk_x dk_y f(k_x,k_y,k_z)$ via

$$f_{1D}(k_z) = \frac{2\pi\hbar}{Vm\omega_z} n_{1D}(z). \quad (1)$$

Here, V is the volume of the uniform trap. Figure 2(a) shows the integrated momentum distribution for different temperatures. Assuming a spherically symmetric momentum distribution, $f_k \equiv f(\mathbf{k}) = f(k)$. Noting that $\int dk_x dk_y f\left(\sqrt{k_x^2+k_y^2+k_z^2}\right) = \pi\int_{k_z^2}^{\infty} d(k^2) f(k)$, the three-dimensional momentum distribution can be obtained from the integrated momentum distribution by differentiation:

$$f_k = -4\pi \frac{df_{1D}(k_z)}{dk_z^2}. \quad (2)$$

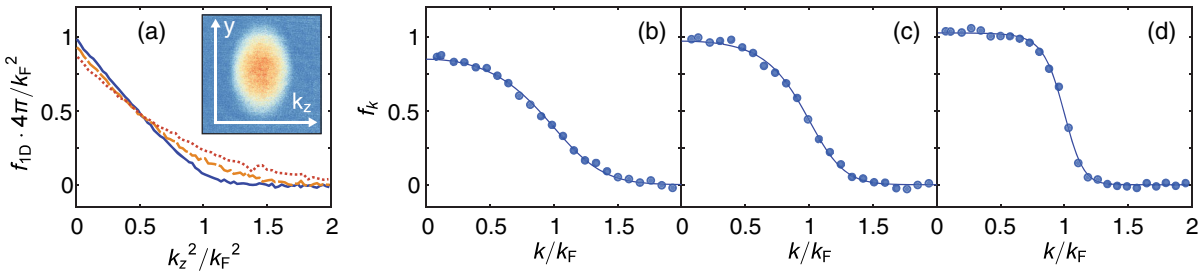

FIG. 2. Momentum distribution of the homogeneous spin-polarized Fermi gas. (a) Doubly integrated momentum distribution f_{1D} for different temperatures in the uniform trap. In order of decreasing temperature: red dotted line, orange dashed line, and blue solid line. Each line corresponds to averages over seven images. The optical density after momentum space mapping along z is shown in the inset. (b),(c),(d) Momentum distribution $f_k = -4\pi d f_{1D}/dk^2$, showing Pauli blocking and Fermi surface formation. Fermi-Dirac fits (solid line) give (b) $T/T_F = 0.49(2)$, (c) $T/T_F = 0.32(1)$, and (d) $T/T_F = 0.16(1)$, with k_F ranging between 2.8 μm^{-1} and 3.7 μm^{-1}. The estimated systematic error in the measurement of f_k is 15%.

As the temperature is lowered, the momentum distribution develops a Fermi surface, and we observe a momentum state occupation of 1.04(15) at low momenta [see Figs. 2(b)–2(d)], where the error in f_k is dominated by the systematic uncertainties in the box volume and the imaging magnification [36]. This is the direct consequence of Pauli blocking and confirms saturation at one fermion per momentum state.

An important motivation for the realization of a homogeneous Fermi gas is the prospect of observing exotic strongly correlated states predicted to exist in narrow parts of the phase diagram, such as the FFLO state [21,22]. In a harmonic trap, such states would be confined to thin isopotential shells of the cloud, making them challenging to observe. We observe pair condensation in a uniformly trapped strongly interacting spin-balanced Fermi gas through a rapid ramp of the magnetic field during time of flight [3,51,52], as shown in Figs. 3(a)–3(c). The pair condensate at the end of the ramp barely expands in time of flight. As a result, the in-trap homogeneity is reflected in a flat top profile of the condensate [see Fig. 3(f)].

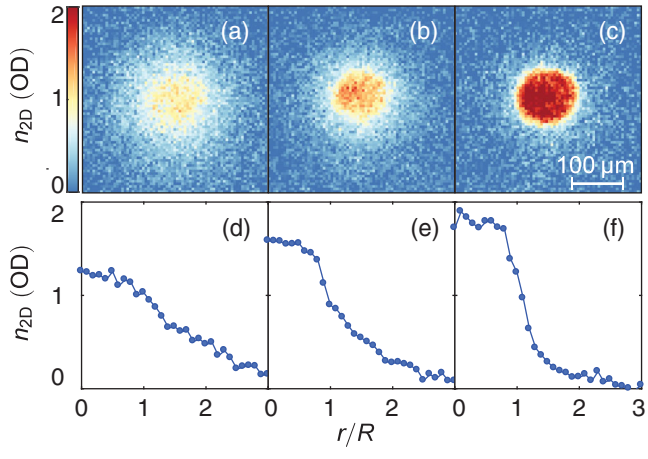

FIG. 3. Pair condensation in the uniform trap. (a), (b), and (c) Absorption images after a rapid ramp of the magnetic field and 10 ms of time of flight. The temperature of the gas is lowered (left to right) by evaporation in the uniform trap. The onset of a bimodal distribution signals the formation of a pair condensate. (d), (e), and (f) show cuts through the images in the top row.

Although a fully uniform potential is ideal for measurements that require translational symmetry, a spatially varying potential can access a large region of the phase diagram in a single experimental run. To harness the advantages of both potentials, we introduce a hybrid geometry that combines the radially uniform cylinder trap with an axially harmonic magnetic trap along the z direction [see Fig. 4(a)]. As a benchmark for the hybrid trap, we perform a thermodynamic study of both a strongly spin-imbalanced and a spin-balanced unitary gas. Figures 4(c)–4(e) display for both cases the y-axis averaged local density, temperature, and compressibility. The data shown in Fig. 4 are extracted from an average of just six images per spin component. For comparison, precision measurements of the equation of state at unitarity, performed in conventional harmonic traps, required averaging of over 100 absorption images [31]. The temperature is obtained from fits to the known equations of state of the noninteracting and spin-balanced unitary Fermi gas, respectively. From the local density in the hybrid trap, we determine the normalized isothermal compressibility $\tilde{\kappa} = \kappa/\kappa_0 = -\partial E_F/\partial U|_T$ for the spin-imbalanced and the spin-balanced gas. Here, U is the external potential, and $\kappa_0 = \frac{3}{2}(1/nE_F)$ is the compressibility of the noninteracting Fermi gas at zero temperature [31].

The strongly spin-imbalanced cloud features two distinct regions in the trap. The center of the cloud is a partially polarized region in which $(n_\uparrow - n_\downarrow)/(n_\uparrow + n_\downarrow) > 0.64$, well above the Clogston-Chandrasekhar limit of superfluidity [53–55]. Surrounding the center is a fully polarized region, where the compressibility is seen to saturate: the real space consequence of the Pauli blocking in momentum space demonstrated in Fig. 2.

The majority spin component in the partially polarized region is affected by the presence of the minority spin component. We measure the compressibility $\tilde{\kappa}_\uparrow = -\partial E_{F\uparrow}/\partial U$ in the partially polarized region, and observe an increase compared to the fully polarized gas. This is expected as

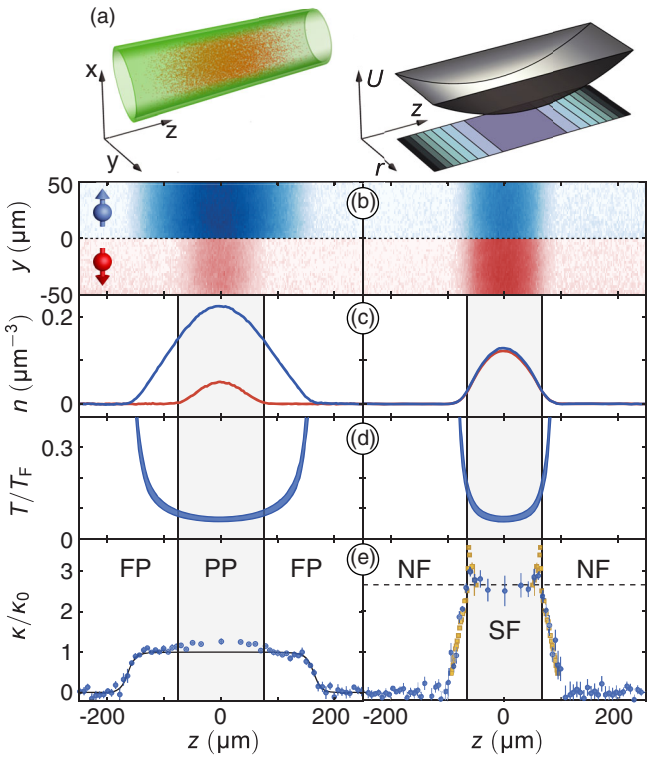

FIG. 4. Unitary Fermi gases in the hybrid trap. (a) Schematic and potential of the trap. The cloud is imaged along an equipotential direction (x axis). Left panels of (b)–(e) show a spin-imbalanced gas above the Clogston-Chandrasekhar limit, whereas the right side corresponds to a spin-balanced gas. The data are averaged over six images. (b) Local density for both spin components, obtained by dividing the column density by the column length. (c) Average density for each x-y equipotential slice. The blue (red) line shows the spin-up (-down) component. (d) Spatially resolved temperature of the gas. The blue shaded region represents the error in the temperature determination. (e) Compressibility of the gas. The solid line in the left panel is the compressibility for an ideal Fermi gas. The crossover from the fully polarized (FP) region to the partially polarized (PP) region is accompanied by an increase in $\tilde{\kappa}$. The yellow squares in the right panel correspond to a precision measurement of the balanced unitary equation of state in the harmonic trap [31]. The peaks in the compressibility signal the phase transition from normal (N) to superfluid (SF). The horizontal dashed line shows the zero-temperature equation of state $\kappa/\kappa_0 = 1/\xi$.

the minority atoms in the center of the trap attract majority atoms and form polarons [7,8]. The effect is indeed predicted by the polaron equation of state [29,30,56]. The observation of this subtle effect highlights the sensitivity of the hybrid potential for thermodynamic measurements.

In the spin-balanced case, κ/κ_0 is significantly larger than for the ideal Fermi gas due to strong interactions. The two prominent peaks in the reduced compressibility signal the superfluid transition at the two boundary surfaces between the superfluid core and the surrounding normal fluid. Near the center of the trap, the reduced compressibility agrees with the $T = 0$ equation of state $\kappa/\kappa_0 = 1/\xi = 2.65(4)$, where ξ is the Bertsch parameter. The shaded region in the right column of Fig. 4 shows the superfluid part of the gas, where the temperature is below the critical temperature for superfluidity $T_c = 0.17T_F$ [31].

The realization of uniform Fermi gases promises further insight into phases and states of matter that have eluded observation or quantitive understanding. This includes the observation of the quasiparticle jump [57] in the momentum distribution of a Fermi liquid, critical fluctuations in the BEC-BCS crossover, and long-lived solitons [58]. Of particular interest are spin imbalanced mixtures that have been studied extensively in harmonic traps [29,30,55,59–62], where the trap drives the separation of normal and superfluid phases into a shell structure. This phase separation should occur spontaneously in a uniform spin-imbalanced gas, possibly forming domains of superfluid and eventually ordering into an FFLO state. In addition, the hybrid potential is a valuable tool for precision measurements that rely on an in-trap density variation. For example, spatially resolved rf spectroscopy [32] in the hybrid potential would measure the homogenous response of the system over a large range of normalized temperatures T/T_F in a single experimental run.

We thank R. Fletcher for a critical reading of the manuscript, and E. A. Cornell and C. Altimiras for helpful discussions. This work was supported by the NSF, the ARO MURI on Atomtronics, AFOSR PECASE and MURI on Exotic Phases, and the David and Lucile Packard Foundation. Z. H. acknowledges support from EPSRC (Grant No. EP/N011759/1).

[1] E. Fermi, Rend. Fis. Acc. Lincei **3**, 145 (1926).
[2] B. DeMarco and D. S. Jin, Science **285**, 1703 (1999).
[3] *Ultra-cold Fermi Gases, Proceedings of the International School of Physics Enrico Fermi, Course CLXIV, Varenna 2006*, edited by M. Inguscio, W. Ketterle, and C. Salomon (IOS Press, Amsterdam, 2008).
[4] S. Giorgini, L. P. Pitaevskii, and S. Stringari, Rev. Mod. Phys. **80**, 1215 (2008).
[5] *The BCS-BEC Crossover and the Unitary Fermi Gas*, edited by W. Zwerger, Lecture Notes in Physics Vol. 836 (Springer-Verlag Berlin Heidelberg, Berlin, Heidelberg, 2012).
[6] M. W. Zwierlein, in *Novel Superfluids* (Oxford University Press, New York, 2014), pp. 269–422.
[7] A. Schirotzek, C.-H. Wu, A. Sommer, and M. W. Zwierlein, Phys. Rev. Lett. **102**, 230402 (2009).
[8] S. Nascimbène, N. Navon, K. J. Jiang, L. Tarruell, M. Teichmann, J. McKeever, F. Chevy, and C. Salomon, Phys. Rev. Lett. **103**, 170402 (2009).
[9] M. Koschorreck, D. Pertot, E. Vogt, B. Fröhlich, M. Feld, and M. Köhl, Nature (London) **485**, 619 (2012).
[10] C. Kohstall, M. Zaccanti, M. Jag, A. Trenkwalder, P. Massignan, G. M. Bruun, F. Schreck, and R. Grimm, Nature (London) **485**, 615 (2012).
[11] R. Jördens, N. Strohmaier, K. Günter, H. Moritz, and T. Esslinger, Nature (London) **455**, 204 (2008).

[12] U. Schneider, L. Hackermüller, S. Will, T. Best, I. Bloch, T. A. Costi, R. W. Helmes, D. Rasch, and A. Rosch, Science **322**, 1520 (2008).

[13] T. Esslinger, Annu. Rev. Condens. Matter Phys. **1**, 129 (2010).

[14] I. Bloch, J. Dalibard, and S. Nascimbène, Nat. Phys. **8**, 267 (2012).

[15] R. A. Hart, P. M. Duarte, T.-L. Yang, X. Liu, T. Paiva, E. Khatami, R. T. Scalettar, N. Trivedi, D. A. Huse, and R. G. Hulet, Nature (London) **519**, 211 (2015).

[16] D. Greif, M. F. Parsons, A. Mazurenko, C. S. Chiu, S. Blatt, F. Huber, G. Ji, and M. Greiner, Science **351**, 953 (2016).

[17] L. W. Cheuk, M. A. Nichols, K. R. Lawrence, M. Okan, H. Zhang, and M. W. Zwierlein, Phys. Rev. Lett. **116**, 235301 (2016).

[18] M. F. Parsons, A. Mazurenko, C. S. Chiu, G. Ji, D. Greif, and M. Greiner, Science **353**, 1253 (2016).

[19] M. Boll, T. A. Hilker, G. Salomon, A. Omran, J. Nespolo, L. Pollet, I. Bloch, and C. Gross, Science **353**, 1257 (2016).

[20] L. W. Cheuk, M. A. Nichols, K. R. Lawrence, M. Okan, H. Zhang, E. Khatami, N. Trivedi, T. Paiva, M. Rigol, and M. W. Zwierlein, Science **353**, 1260 (2016).

[21] A. J. Larkin and Y. N. Ovchinnikov, Zh. Eksp. Teor. Fiz. **47**, 1136 (1964).

[22] P. Fulde and R. A. Ferrell, Phys. Rev. **135**, A550 (1964).

[23] L. Radzihovsky and D. E. Sheehy, Rep. Prog. Phys. **73**, 076501 (2010).

[24] A. L. Gaunt, T. F. Schmidutz, I. Gotlibovych, R. P. Smith, and Z. Hadzibabic, Phys. Rev. Lett. **110**, 200406 (2013).

[25] T. F. Schmidutz, I. Gotlibovych, A. L. Gaunt, R. P. Smith, N. Navon, and Z. Hadzibabic, Phys. Rev. Lett. **112**, 040403 (2014).

[26] N. Navon, A. L. Gaunt, R. P. Smith, and Z. Hadzibabic, Science **347**, 167 (2015).

[27] L. Chomaz, L. Corman, T. Bienaimé, R. Desbuquois, C. Weitenberg, S. Nascimbène, J. Beugnon, and J. Dalibard, Nat. Commun. **6**, 6162 (2015).

[28] T.-L. Ho and Q. Zhou, Nat. Phys. **6**, 131 (2009).

[29] S. Nascimbène, N. Navon, K. J. Jiang, F. Chevy, and C. Salomon, Nature (London) **463**, 1057 (2010).

[30] N. Navon, S. Nascimbene, F. Chevy, and C. Salomon, Science **328**, 729 (2010).

[31] M. J. H. Ku, A. T. Sommer, L. W. Cheuk, and M. W. Zwierlein, Science **335**, 563 (2012).

[32] Y.-I. Shin, C. H. Schunck, A. Schirotzek, and W. Ketterle, Phys. Rev. Lett. **99**, 090403 (2007).

[33] A. Schirotzek, Y.-I. Shin, C. H. Schunck, and W. Ketterle, Phys. Rev. Lett. **101**, 140403 (2008).

[34] J. H. McLeod, J. Opt. Soc. Am. **44**, 592 (1954).

[35] I. Manek, Y. Ovchinnikov, and R. Grimm, Opt. Commun. **147**, 67 (1998).

[36] See Supplemental Material at http://link.aps.org/supplemental/10.1103/PhysRevLett.118.123401 for further information on making and characterizing the uniform trap, optical pumping for the momentum-space mapping, and calibrating the absorption imaging.

[37] R. Thomas, K. O. Roberts, E. Tiesinga, A. C. J. Wade, P. B. Blakie, A. B. Deb, and N. Kjærgaard, Nat. Commun. **7**, 12069 (2016).

[38] A. G. Truscott, K. E. Strecker, W. I. McAlexander, G. B. Partridge, and R. G. Hulet, Science **291**, 2570 (2001).

[39] F. Schreck, L. Khaykovich, K. L. Corwin, G. Ferrari, T. Bourdel, J. Cubizolles, and C. Salomon, Phys. Rev. Lett. **87**, 080403 (2001).

[40] B. DeMarco, S. B. Papp, and D. S. Jin, Phys. Rev. Lett. **86**, 5409 (2001).

[41] A. Sommer, M. Ku, and M. W. Zwierlein, New J. Phys. **13**, 055009 (2011).

[42] T. Rom, T. Best, D. van Oosten, U. Schneider, S. Fölling, B. Paredes, and I. Bloch, Nature (London) **444**, 733 (2006).

[43] T. Müller, B. Zimmermann, J. Meineke, J.-P. Brantut, T. Esslinger, and H. Moritz, Phys. Rev. Lett. **105**, 040401 (2010).

[44] C. Sanner, E. J. Su, A. Keshet, R. Gommers, Y.-I. Shin, W. Huang, and W. Ketterle, Phys. Rev. Lett. **105**, 040402 (2010).

[45] A. Omran, M. Boll, T. A. Hilker, K. Kleinlein, G. Salomon, I. Bloch, and C. Gross, Phys. Rev. Lett. **115**, 263001 (2015).

[46] T. E. Drake, Y. Sagi, R. Paudel, J. T. Stewart, J. P. Gaebler, and D. S. Jin, Phys. Rev. A **86**, 031601 (2012).

[47] I. Shvarchuck, C. Buggle, D. S. Petrov, K. Dieckmann, M. Zielonkovski, M. Kemmann, T. G. Tiecke, W. von Klitzing, G. V. Shlyapnikov, and J. T. M. Walraven, Phys. Rev. Lett. **89**, 270404 (2002).

[48] A. H. van Amerongen, J. J. P. van Es, P. Wicke, K. V. Kheruntsyan, and N. J. van Druten, Phys. Rev. Lett. **100**, 090402 (2008).

[49] S. Tung, G. Lamporesi, D. Lobser, L. Xia, and E. A. Cornell, Phys. Rev. Lett. **105**, 230408 (2010).

[50] P. A. Murthy, D. Kedar, T. Lompe, M. Neidig, M. G. Ries, A. N. Wenz, G. Zürn, and S. Jochim, Phys. Rev. A **90**, 043611 (2014).

[51] C. A. Regal, M. Greiner, and D. S. Jin, Phys. Rev. Lett. **92**, 040403 (2004).

[52] M. W. Zwierlein, C. A. Stan, C. H. Schunck, S. M. F. Raupach, A. J. Kerman, and W. Ketterle, Phys. Rev. Lett. **92**, 120403 (2004).

[53] B. S. Chandrasekhar, Appl. Phys. Lett. **1**, 7 (1962).

[54] A. M. Clogston, Phys. Rev. Lett. **9**, 266 (1962).

[55] M. W. Zwierlein, A. Schirotzek, C. H. Schunck, and W. Ketterle, Science **311**, 492 (2006).

[56] Y.-I. Shin, Phys. Rev. A **77**, 041603 (2008).

[57] G. D. Mahan, *Many-Particle Physics* (Springer, Boston, MA, 2000).

[58] M. J. H. Ku, B. Mukherjee, T. Yefsah, and M. W. Zwierlein, Phys. Rev. Lett. **116**, 045304 (2016).

[59] G. B. Partridge, W. Li, R. I. Kamar, Y.-A. Liao, and R. G. Hulet, Science **311**, 503 (2006).

[60] Y.-I. Shin, M. W. Zwierlein, C. H. Schunck, A. Schirotzek, and W. Ketterle, Phys. Rev. Lett. **97**, 030401 (2006).

[61] Y.-I. Shin, C. H. Schunck, A. Schirotzek, and W. Ketterle, Nature (London) **451**, 689 (2008).

[62] Y.-A. Liao, A. S. C. Rittner, T. Paprotta, W. Li, G. B. Partridge, R. G. Hulet, S. K. Baur, and E. J. Mueller, Nature (London) **467**, 567 (2010).